Hydrol. Earth Syst. Sci. Discuss., 5, 2425–2457, 2008
www.hydrol-earth-syst-sci-discuss.net/5/2425/2008/

Hydrology and Earth System Sciences Discussions

Papers published in *Hydrology and Earth System Sciences Discussions* are under open-access review for the journal *Hydrology and Earth System Sciences*

Quantifying the effect of land use and land cover change on green water and blue water in northern part of China

X. Liu[1], L. Ren[1], F. Yuan[1], V. P. Singh[2], X. Fang[1], Z. Yu[1], and W. Zhang[1]

[1]State Key Laboratory of Hydrology, Water Resources and Hydraulic Engineering, College of Hydrology and Water Resources, Hohai University, No. 1 Xikang Road, Nanjing 210 098, The P. R. China
[2]Department of Biological and Agricultural Engineering, Texas A and M University, 2117 TAMU, College Station, Texas 77 843–2117, USA

Received: 9 July 2008 – Accepted: 18 July 2008 – Published: 29 August 2008

Correspondence to: X. Liu (liuxiaofanhhu@yahoo.com.cn)

Published by Copernicus Publications on behalf of the European Geosciences Union.

Abstract

In order to investigate the effect of land use and land cover changes on hydrological process in northern parts of China, a distributed hydrological model was developed and applied in the Laohahe catchment. The direct evaporation from the intercepted water, potential canopy transpiration and potential soil evaporation were computed using a physically-based two-source potential evapotranspiration model, which would be regarded as input to the distributed hydrological model for the computation of actual evaportranspiration. Runoff generation was based on mixed runoff mechanisms of infiltration excess runoff and saturation excess runoff and the Muskingum-Cunge method was adopted for flow routing. The land cover data were available for 1980, 1989, 1996 and 1999. Daily streamflow measurements were available from 1964 to 2005 and were divided into 4 periods: 1964–1979, 1980–1989, 1990–1999 and 2000–2005, based on the land cover scenarios. The distributed hydrological model was coupled with a two-source potential evaportranspiration model for simulating daily runoff. The result of runoff simulation showed that the saturation excess runoff generation was dominant in the catchment. Model parameters were calibrated using hydrometeorological and land cover data corresponding to the same period. Streamflow simulation was conducted for each period under these four land cover scenarios. The results showed that the change of land use and land cover had a significant influence on evapotranspiration and runoff. The land cover data showed that forest land and water body had decreased from 1980 through 1999 and farm land and grass land had increased. This change caused the vegetation interception evaporation and vegetation transpiration to decrease, whereas the soil evaporation tended to increase. Thus the green water decreased but the blue water increased over the Laohahe catchment. This result was inconsistent with the fact that runoff ratio had a tendency of decrease in the catchment in 2000. It is this reason that water use out of stream channel has been increasing in recent years.

1 Introduction

Water is always on the move in the hydrological cycle. It is the very foundation for all biological life on earth, and the basic link between the biosphere and the anthroposphere (Falkenmark and Rockstrom, 2004). Blue water is visible liquid water moving above and below the ground as surface or groundwater runoff, respectively (FAO, 1995b, 1997). Blue water can thus be in the form of surface runoff in rills, gullies and rivers, or water stored in reservoirs and lakes, or water flowing underground, recharging water tables and aquifers. Green water is defined as the invisible vapour moving to the atmosphere (FAO, 1995, 1997), including productive green water defined as transpiration from plants and trees, and nonproductive green water consisting of soil evaporation and interception evaporation. Green water thus equates the commonly used term evapotranspiration, which combines productive and non-productive vapour in one term. It is a new concept to divide water into blue water and green water, which may effectively be utilized to study the effect of land use and land cover changes on the catchment water balance.

Quantification of the effect of land use and land cover changes on the partition of blue water and green water of a river basin has been an area of interest to hydrologists in recent years. However, the conversion of rainfall into runoff is complex and our understanding of the quantitative relationship between the land cover properties and runoff generation mechanism is less than complete.

The effect of land use and land cover changes on the hydrological processes is mainly represented by the changes in vegetation interception, soil evaporation, plant transpiration, infiltration and soil water content, and consequently changes in the partition of blue water and green water from rainfall. In earlier studies, the assessment of the impact of land use and land cover changes on runoff was done mainly through field experiments. There are many reviews of these experiments in the literature, notably those of Hibbert (1967), Hollis (1975), Bosch and Hewlett (1982), and Zhang et al. (1999). These studies, which generally indicate that deforestation causes an increase in the

mean annual discharge, have concentrated on the impacts of forest management on water yield (Siriwardena et al., 2006). While field experiments can conclusively demonstrate the consequences of land use and land cover changes, modeling studies often provide more insight into the flow mechanisms and processes. Modeling studies have an advantage over field experimental studies by being more flexible and rigorous in experimental design and enabling mechanistic interpretations. Besides, models are able to yield results quickly with much less cost and time (Li et al., 2007).

Nowadays, hydrological models are being used to address the impact of land use and land cover changes. Lorup et al. (1998) calibrated lumped models for a reference period when there is little change in land cover and applied it to a subsequent period in which changes in land cover have taken place. They carried out trend analysis of the bias between modeled and observed runoff to investigate changes in catchment runoff that might arise due to the land cover change. Wilk et al. (2001) calibrated a daily rainfall-runoff model for the pre-clearing period and then used it to predict the catchment yield after clearing. They were unable to detect any hydrological change that could be attributed to the reduction in forest cover. They attributed this to the fact that the land use and land cover changes were not uniform across the catchment and there was a significant number of trees remaining on agricultural land and secondary re-growth on agricultural plots. Chen et al. (2004) applied a distributed hydrological model SWAT to simulate the rainfall-runoff relationship of the Suomo basin under different land covers in order to evaluate the impact of land cover changes on runoff, evapotranspiration and peak flow. They found that if the land cover changed from a non-vegetation-cover to a full-forest-cover scenario, the runoff depth (blue water) decreased and evaporation (green water) increased. With the same recurrent flood flow, the peak flow value under full-forest-cover scenario was 31.2% less than that under non-vegetation-cover scenario.

The objective of this paper was to investigate the effect of land use and land cover changes on the hydrological processes of Laohahe Catchment in northern China, using a distributed hydrological model coupled with a two-source potential evapotranspi-

ration model. Using the direct evaporation from the intercepted water, potential canopy transpiration and potential soil evaporation as the input to the distributed hydrological model, the effect of land cover change on the evapotranspiration process was quantified. Four land cover scenarios obtained by remote sensing were used to represent the vegetative cover over the catchment during four periods: 1964–1979, 1980–1989, 1990–1999 and 2000–2005, respectively. Model parameters were calibrated using hydrometeorological and land cover data corresponding to the same period. The effect of land cover changes was then modeled by applying the model to three other land cover scenarios.

2 Study area and data preparation

2.1 Description of the study area

The Laohahe catchment, with a total drainage area of 7720 km^2, is controlled by Taipingzhuang hydrological station (42°12′ N, 119°15′ E) and is situated in northern China. The river across the basin is the upstream tributary of the Laohahe River, as shown in Fig. 1. The main production approaches are agriculture and stock raising in the catchment, thus grass land and crop land are the dominant vegetations. The major driving force of land cover and land use change is increases in population and direction of national development polices. Since the foundation of China, there were four times large-scale reclamation in the catchment, however conversion of cropland to forest or grassland was also progressing at the same time. Elevation within the catchment ranges from 444 m to 1836 m above mean sea level, with elevation declining from southwest toward northeast. There are 19 rain gauges, 4 meteorological stations and 1 hydrological station (Taipingzhuang) in this basin and the recorded data are available from 1964 to 2005. Annual average maximum (minimum) temperature is 14°C (2°C) ranging from −4(−16) in January to 29(18) in July. The average annual precipitation is approximately 451 mm, and the spatial and temporal distribution of precipitation is

uneven. About 88% of the annual precipitation occurs during the months from May through September. Thus Laohahe catchment lies in a semi-arid region in northern China.

2.2 Data preparation

2.2.1 Topography

The digital elevation model (DEM) data (Fig. 2) within 40.9° ~42.9° N and 117.2° ~120° E at the spatial resolution of 30 s by 30 s were obtained from the Global Land One-kilometer Base Elevation database. The river network and catchment boundary were automatically generated by the digital elevation drainage network model (Martz and Garbrecht, 1992).

2.2.2 Land use and land cover data

Four scenarios of land cover maps (Fig. 3) at the spatial scale of DEM were obtained by remote sensing and were available to represent the vegetative cover over the catchment during the period of 1964–2005. These land cover maps were interpreted from Landsat MSS, TM and ETM+ images with a variety of reference data. Decision tree classification method was used here based on the analyzed spectral characteristics and the spatial patterns of land cover classes. All the user's and producer's accuracies of the classification were respectively above 87.7% and 86.9%, and the overall accuracies were above 90.6%, and Kappa statistic were above 90.9%.The vegetation was classified into 3 types: the gross, namely forest land, grass land, and crop land.

2.2.3 NDVI data

The NOAA-AVHRR NDVI dataset is available monthly for the globe at an interval of 8 km, covering the period from July of 1981 to September 2001, except for the data-missing period from September to December 1994. The basin part of NDVI was clipped

using the basin boundary and transferred into the Lambert Azimuthal Equal Area projection and the resolution of 30 s in Arc/Info software.

2.2.4 Meteorological data

The required meteorological data include daily mean, maximum and minimum air temperature; air vapor pressure; wind velocity; daylight duration; and precipitation. In this study, daily precipitation data were obtained from 19 rainfall gauge stations spread across the catchment, and other meteorological data were obtained from 4 meteorological stations around the catchment. Based on DEM, the key meteorological variables were topographically corrected with the empirical relationships extracted by data for the entire Laohahe catchment:

$$T_a = -0.586 Z_{100} + T_{\text{obs}} \quad (1)$$

$$e_a = e_{\text{obs}} \exp(-0.0507 Z_{100}) \quad (2)$$

$$u_a = u_{\text{obs}} \{3.6 - 2.6 \exp(-0.0569 Z_{100})\} \quad (3)$$

where Z_{100} is the altitude difference between grid cell and meteorological station in 100 m; and the quantities T_{obs}, e_{obs}, u_{obs} are the air temperature, air vapor pressure and wind speed records at the meteorological station, respectively. All meteorological data were interpolated over the whole study area using the inverse distance square method (Ashraf et al., 1997).

3 Model description

3.1 Two-source potential evapotranspiration model

Evapotranspiration is a process of water vapor transfer from the wet soil-vegetation system to the dry atmosphere, including interception evaporation, soil evaporation, and

plant transpiration. Potential evapotranspiration, PET, is generally considered to be the amount of water which would be lost to the atmosphere from a land surface where water is enough to satisfy the atmospheric evaporation demand.

Mo et al. (2004) developed a two-source evapotranspiration model based on the Penman-Monteith equation for actual evapotranspiration:

$$E_c = \frac{\Delta R_{nc} + \frac{\rho C_p D_0}{r_{ac}}}{\lambda[\Delta + \gamma(1 + \frac{r_c}{r_{ac}})]}(1 - W_{fr}) \quad (4)$$

$$E_s = \frac{\Delta(R_{ns} - G) + \frac{\rho C_p D_0}{r_{as}}}{\lambda[\Delta + \gamma(1 + \frac{r_s}{r_{as}})]} \quad (5)$$

$$E_i = \frac{\Delta R_{nc} + \frac{\rho C_p D_0}{r_{ac}}}{\lambda(\Delta + \gamma)} W_{fr} \quad (6)$$

where E_c, E_i and E_s are the canopy transpiration, evaporation from the intercepted water, and soil evaporation, respectively; R_{nc} and R_{ns} are the net radiation absorbed by canopy and soil (Wm^{-2}), respectively; G is the soil heat flux (Wm^{-2}); λ is the latent heat of vaporization ($MJ\,kg^{-1}$); ρ is the air density ($kg\,m^{-3}$); C_p is the air specific heat at constant pressure ($KJ\,kg^{-1}\ ^\circ C^{-1}$); γ is the psychrometric constant ($kPa\,^\circ C^{-1}$); Δ is the first-order derivative of saturation vapor pressure with temperature ($kPa\,^\circ C^{-1}$); W_{fr} is the wetted fraction of the canopy; r_c, r_s, r_{ac} and r_{as} are the bulk stomatal resistance of canopy, soil surface resistance, bulk boundary-layer resistance of the canopy, and aerodynamic resistance between the soil surface and canopy air space, respectively($s\,m^{-1}$); and D_0 is water vapor deficit at the source height (kPa).

For calculating the potential evapotranspiration consisting of potential canopy transpiration, potential soil evaporation and direct evaporation from the intercepted water,

Yuan (2006) improved the two-source evapotranspiration model:

$$E_{pc}=\frac{\Delta R_{nc}+\frac{\rho C_p D_0}{r_{ac}}}{\lambda[\Delta+\gamma(1+\frac{r_{cp}}{r_{ac}})]}(1-W_{fr}) \quad (7)$$

$$E_{ps}=\frac{\Delta(R_{ns}-G)+\frac{\rho C_p D_0}{r_{as}}}{\lambda[\Delta+\gamma(1+\frac{r_{sp}}{r_{as}})]} \quad (8)$$

where E_{pc} is the potential canopy transpiration, E_{ps} is the potential soil evaporation, r_{cp} is the bulk stomatal resistance of canopy while the soil moisture at field capacity, and r_{sp} is the soil surface resistance while the soil moisture at field capacity. In this study, r_{sp}=300 s m^{-1}.

The method of calculating evaporation from the intercepted water is the same as Eq. (6). The detailed parameterization schemes of radiation balance, land surface resistance and interception in the two-source potential evapotranspiration model can be referred to the paper by Yuan et al. (2008).

The evaporation from water surface estimated by substituting the aerodynamic resistance of Penman wind speed function and r_s=0 into P-M equation (Shuttleworth, 1993) was also considered in this study:

$$ET=\frac{\Delta}{\Delta+\gamma}0.408(R_n-G)+\frac{\gamma}{\Delta+\gamma}2.624(1+0.536u_2)(e_s-e_a) \quad (9)$$

where e_s and e_a are the saturation and actual vapour pressures (kPa), respectively; and u_2 is the wind speed (m s^{-1}) at 2 m height.

3.2 Hydrological model

Potential evapotranspiration was used to drive a grid-based distributed hydrological model. The evapotranspiration component was represented by a model of three soil

layers (Zhao, 1992). Runoff generation was based on a hybrid runoff model (Hu, 1993), and runoff routing was carried out using the Muskingum-Cunge method.

Numerous field studies show that runoff within a basin is mainly generated by two mechanisms: infiltration excess (Horton) runoff and saturation excess (Dunne) runoff. The hybrid runoff model combines the two runoff mechanisms by means of the combination of spatial distribution curve of soil tension water storage capacity and that of infiltration capacity. This is the way daily runoff simulation and flood forecasting were done in Laohahe catchment.

The basic concept of the hybrid runoff model can be expressed as shown in Fig. 4. The blue curve represents the distribution curve of soil tension water storage capacity regarding the alpha axis as the abscissa. For a catchment, the distribution curve of soil tension water storage capacity is unique. The pink curve represents the distribution curve of soil infiltration capacity regarding the beta axis as the abscissa. The distribution curve of soil infiltration capacity isn't unique, which related with the soil moisture content. So the two curves meet in different fields or don't meet for different soil moisture content and precipitation.

The basin is spatially divided by the distribution curve of soil tension water storage capacity into two parts, α and $(1-\alpha)$. The rainfall over the sub-area, α, all becomes runoff, including surface runoff and groundwater runoff. Over the other sub-area, $(1-\alpha)$, runoff could not be produced until the soil tension water storage equaled field capacity. In the process of soil moisture content up to its field capacity, surface runoff may be possibly generated when rainfall intensity exceeds infiltration rate over a partial area where soil moisture does not reach its field capacity. That partial area is shown as the shaded area in Fig. 5a. The distribution curve of the tension water storage capacity can be written as follows:

$$\alpha = 1 - (1 - \frac{W'}{W'_m})^B \tag{10}$$

where abscissa variable α denotes the proportional fraction of the pervious area in the whole basin area, in which tension water storage capacity is equal to or less than the

ordinate value, W'. W'_m is the maximum value of tension water capacity at a point within the studied basin. Parameter B is the exponential of the parabolic curve. Following Zhao (1980), the areal mean tension water capacity W_m can be expressed as:

$$W_m = \frac{W'_m}{1+B} \tag{11}$$

The basin is spatially segmented by the distribution curve of soil infiltration capacity into two parts, β and $(1-\beta)$. Surface runoff is produced over the partial area, β, when rainfall intensity exceeds infiltration rate; runoff can not be generated over the other area, $(1-\beta)$, for the rainfall intensity is less than the infiltration rate. However, in spite of weak rain intensity, runoff would probably be generated over the partial area of $(1-\beta)$, where soil moisture content has reached its field capacity. That partial area is represented as the shaded area in Fig. 5b. The Horton infiltration curve was adopted for the computation of infiltration rate at any point within the basin, which can be expressed as:

$$f_t = f_c + (f_0 - f_c)e^{-kt} \tag{12}$$

where f_t is the point value of infiltration rate at time t; f_0 is the maximum infiltration rate; and f_c the static infiltration constant at a surface point; and k is decay coefficient with time. The spatial distribution curve of infiltration quantity during the time step of Δt can be expressed as:

$$\beta = 1 - \left(1 - \frac{F'_{\Delta t}}{F'_{m\Delta t}}\right)^{BX} \tag{13}$$

where variable β is the fraction of an area for which infiltration quantity is equal to or less than $F'_{\Delta t}$; $F'_{\Delta t}$ and $F'_{m\Delta t}$ are the point values of infiltration quantity and the maximum infiltration quantity in the duration of Δt, respectively; and BX is the shape parameter.

The average spatial infiltration quantity, $F_{m\Delta t}$, similar to the case of tension water capacity, can be computed as:

$$F_{m\Delta t}=\frac{F'_{m\Delta t}}{1+BX} \tag{14}$$

The runoff generation calculation of HYB was introduced in detail by Ren et al. (2008).

4 Model calibration and validation

Since the hybrid runoff model is a conceptual model, its 11 parameters had to be estimated through model calibration against observed catchment response. The performance of the model is measured on a daily time step using the Nash-Sutcliffe efficiency (DC, Eq. 15) and relative error (Bias, Eq. 16). The results of model calibration during the 4 periods using the corresponding hydrometeorological data and land cover data are shown in Table 1.

$$DC=1-\frac{\sum_{i=1}^{N}(Q_{\mathrm{obs}_i}-Q_{sim_i})^2}{\sum_{i=1}^{N}(Q_{\mathrm{obs}_i}-\overline{Q_{\mathrm{obs}_i}})^2} \tag{15}$$

$$\mathrm{Bias}=\frac{\sum_{i=1}^{N}Q_{sim_i}-\sum_{i=1}^{N}Q_{\mathrm{obs}_i}}{\sum_{i=1}^{N}Q_{\mathrm{obs}_i}}\times 100\% \tag{16}$$

where Q_{obs_i} is observed streamflow at time step i, Q_{sim_i} is the simulated streamflow at time step i, $\overline{Q_{\mathrm{obs}_i}}$ is the mean of the observed values, and N is the number of data points.

In Table 2, the best performance appears for the period of 1964–1979, while during the period of 2000–2003, the simulated discharge is much larger than the observed one. In the Laohahe catchment, the effect of human activities on streamflow has intensified since 1980. Ren et al. (2002) found that the amount of streamflow in northern China has a decreasing tendency in terms of natural basins and administrative regions. The increase of water use outside the stream channel is the primary reason, besides climate change, for the decrease of streamflow. The better simulated result of daily discharge (DC=0.834, Bias=−8.46%) is in the year 1979, and the worst simulated result (DC=−1319.7, Bias=195.9%) is in the year of 2004 during the period of 1964–2005. Figure 6 shows the comparison of the observed and simulated streamflow in the two years. 1979 is a wet year, annual precipitation of which is 586 mm, while the annual precipitation of 2004 is only 418 mm. Due to more intense human activities (i.e. reservoir filling, water use outside stream channel) in the dry year, it is difficult to simulate the runoff in the dry year. For example, after July 2004 the observed discharge kept low, even though there are plenty of precipitation in the corresponding period (Fig. 6).

5 Results and discussion

5.1 Land use and land cover changes since 1980

For applying the distributed hydrological model, the original land use data were upscaled to the resolution of 30 s and reclassification. These processes reduced the precision of land use data at a certain extent. The percentages of the main vegetation types from 4 land cover maps are shown in Table 3 which shows important changes in land use and land cover during the period of interest. The main land cover types are forest land, grass land and crop land, which account for more than 95% of the total area. The variation of land use and land cover in Laohahe catchment is complex from 1980 to 1999, and it is difficult to discern a consistent trend of change. Nevertheless, for the whole, the forest land decreased from 25.9% of the area in 1980 to 10.5% in

1999, despite the increase to 31.6% in 1996; grass land and crop land both have the increasing tendency.

5.2 Quantitative effect of land use and land cover changes on green water

Green water defined as above is the evapotranspiration from the moist land surface into atmosphere. Incoming rainfall is partitioned into green water and blue water in the hydrological cycle. Land cover and soil characteristics can influence the rainfall partition.

Daily direct evaporation from the intercepted water, potential canopy transpiration and potential soil evaporation during 4 periods were computed using the two-source potential evapotranspiration model under 4 land cover scenarios. Table 4 presents the calculated mean annual values. In this table, the shaded portions show the results that were calculated from the corresponding land cover data and hydrometeorological data. Potential evapotranspiration (PET) is equal to the sum of direct evaporation from the intercepted water (E_i), potential canopy transpiration (E_{pc}) and potential soil evaporation (E_{ps}). Comparing the shaded results for the period of 1964–1979 and period 1990–1999, the mean annual PET for the latter period is larger than that for the former period by 12.2 mm. Comparing the results between the period of 1964–1979 and period 1990–1999 both under the 1980 land cover scenario, the latter mean annual PET is larger than the former one only by 0.9 mm, which may be regarded as the cause of climate change. Comparing the results for the period of 1990–1999 under the 1980 and 1996 land cover scenarios, the latter mean annual PET is larger than the former one by 11.3 mm. This difference is caused by land cover changes. Thus, one can conclude that land cover change is the dominant factor of the PET change between the periods of 1964–1979 and 1990–1999. Comparing the results during the period of 1964–1979 under the 1980 and 1996 land cover scenarios, the latter mean annual interception evaporation is larger than the former one by 18.3 mm, and the latter mean annual potential canopy transpiration is larger than the former one by 69.3 mm, the latter mean annual potential soil evaporation is smaller than the former one by 73.7 mm and the

latter actual evapotranspiration (E_a) is larger than the former one by 4 mm. From 1980 to 1996, the forest land increased from 25.9% to 31.6%, the grass land decreased from 29.1% to 16.1%, and the crop land increased from 42.7% to 48% (Table 3). Thus the change of grass land into forest land and crop land in the Laohahe catchment caused the increment in mean annual interception evaporation and potential canopy transpiration, the reduction in mean annual potential soil evaporation, and the increment in mean annual potential evapotranspiration and actual evapotranspiration. The similar results were obtained in changing the present land use into the scenario for natural conditions with complete tree cover by Ott and Uhlenbrook (2004). Similarly comparing the results over the period of 1990–1999 under the 1996 and 1999 land cover scenarios, one can conclude that the change of forest land and crop land into grass land in Laohahe catchment caused the reduction in mean annual interception evaporation and potential canopy transpiration, the increment in mean annual potential soil evaporation, and the reduction in mean annual potential evapotranspiration and actual evapotranspiration. Since actual evapotranspiration depends not only on potential evapotranspiration but also on precipitation, the degree of change of actual evapotranspiration attributed to land cover changes is slighter than that of potential evapotranspiration in the Laohahe catchment.

Comparing Fig. 7 with Fig. 3, the distribution of mean annual PET is greatly influenced by the land cover data. The area with forest land can have a larger mean annual PET, and the area with the grass land can have a smaller mean annual PET over the Laohahe catchment. Taking the 1999 land cover scenario as an example, the mean annual PET of forest land, grass land and crop land over the period of 1980–1999 was 772.1 mm, 715.4 mm and 753.2 mm, respectively.

5.3 Quantitative effect of land use and land cover changes on blue water

Blue water defined as above is surface or groundwater runoff moving above and below the ground, respectively. Daily runoff for the period of 1964–2005 was simulated by the distributed hydrological model under the 4 land cover scenarios. Table 5 presents

the simulated mean annual surface runoff, groundwater runoff and total runoff during each period under those 4 land cover scenarios. The observed annual precipitation and runoff during the 4 periods were shown in Table 6.

The shaded portions in Table 5 are the results that were simulated through the corresponding land cover data and hydrometeorological data. The simulated surface runoff is only about 13% of the total runoff during the period of 1964–2005. The effect of land use and land cover changes on the blue water (runoff) is contrary to the green water (evapotranspiration), because the sum of green water and blue water should be equal to the incoming rainfall in the hydrological cycle from an average viewpoint.

As land cover changes from 1980 to 1996, with the grass land changing into forest land and crop land in the catchment, not only surface runoff but also groundwater runoff decreased during the period of 1964–1979. The quantitative changes in land use and land cover from 1980 to 1996 are that the grass land decreased by 1004 km^2, the forest land increased by 440 km^2 and the crop land increased by 409 km^2. The runoff ratio decreased from 0.0981 to 0.0896. When land cover changes from 1980 to 1999, with the forest land changing into the grass land in the catchment, surface runoff and groundwater runoff increased for the period of 1964–1979. The quantitative changes in land use and land cover from 1980 to 1999 are that grass land increased by 1343 km^2, forest land decreased by 1189 km^2, and crop land increased by 15 km^2. The runoff ratio increased from 0.0981 to 0.0995, increased only by 1.4%. From these two results, one can conclude that the effect of land use and land cover changes on runoff is non-linear.

The larger difference between simulated runoff and observed runoff for the period of 2000–2005 (Tables 5 and 6) may be a result of the water use out of the river channel.

6 Conclusions

The purpose of this study was to assess the quantitative effect of land use and land cover changes on green water and blue water in the Laohahe Catchment using a

distributed hydrological model coupled with a two-source potential evapotranspiration model. The observed daily hydrometeorological data from 1964 to 2005 was divided into 4 periods: 1964–1979, 1980–1989, 1990–1999 and 2000–2005. The land cover scenarios for those four periods were developed using the land cover data in 1980, 1989, 1996 and 1999, respectively. The variation of land use and land cover in Laohahe catchment is complex from 1980 to 1999. For the whole, the forest land decreased from 25.9% of the area in 1980 to 10.5% in 1999, despite the increase to 31.6% in 1996; grass land and crop land both have an increasing tendency.

Model calibration during those 4 periods using the corresponding hydrometeorological data and land cover data was initially carried out. The performance of this distributed hydrological model was better in the wet year than in the dry one. The proportions of the surface runoff and groundwater runoff simulated indicated that the saturation runoff generation was dominant in the Laohahe catchment.

The annual interception evaporation, potential canopy transpiration, potential soil evaporation and actual evapotranspiration in 4 periods under each land cover scenario show that land cover change is the dominant factor for the change of potential evapotranspiration between the periods of 1964–1979 and 1990–1999, and the change of forest land and crop land into grass land in Laohahe catchment caused the reduction in annual interception evaporation and potential canopy transpiration, the increment in annual potential soil evaporation, and the reduction in mean annual potential evapotranspiration and actual evapotranspiration. Due to the actual evapotranspiration depending not only on the potential evapotranspiration but also on precipitation, the degree of change of actual evapotranspiration attributed to land cover changes is slighter than that of potential evapotranspiration in the Laohahe Catchment. The distribution map of mean annual PET over the Laohahe catchment showed that the area with forest land can have a larger mean annual PET, and the area with the grass land can have a smaller mean annual PET.

The effect of land use and cover changes on the blue water (runoff) is contrary to that on the green water (evapotranspiration). When land cover changed from 1989 to

1999, the blue water during the period of 1980–1989 was increased by 2.6%, which is inconsistent with the fact that the runoff ratio for the period of 2000–2005 was less than that for the period of 1980–1989, even though the values of precipitation for both periods are comparable (Table 6).

In general, the change of land use and land cover change situation is not continuous, and is small in consecutive years. However, the change is quite large on a decadal basis. In this study, according to the availability of land use data, four scenarios of land use and land cover were selected for representing the vegetation cover over the studied area during four different periods. This presentation has error, to some extent. The analyses remarked above imply that four scenarios can represent the situation of land use and land cover in the corresponding periods, respectively. Excluding the input data error, the model parameters equifinality problem, simplifications inherent in the model structure and mathematical descriptions of various processes could lead to the uncertainty of model results (Ott and Uhlenbrook, 2004). In order to get more accurate, reliable model results, more spatially and temporally distributed data (land use data, meteorological data) should be obtained by remote sensing or field investigation, and the hydrological physical processes(evapotranspiration, infiltration, runoff generation and runoff concentration) should be understand deeply, especially in the semi-arid area.

Acknowledgements. This study was supported by the National Key Basic Research Program of China under Project No. 2006CB400502. Also this research is the result of the 111 Project under Grant B08048, Ministry of Education and State Administration of Foreign Experts Affairs, P. R. China. This work was also supported by the Program for Changjiang Scholars and Innovative Research Team in University under Grant No. IRT0717, Ministry of Education, China and the Grand Sci-Tech Research Project of Ministry of Education under Grant No. 308012.

References

Ashraf, M., Loftis, J., and Hubbard, K. G.: Application of geostatistics to evaluate partial weather station networks, Agr. Forest Meteorol., 84, 255–271, 1997.

Bosch, J. M. and Hewlett, J. D.: A review of catchment experiments to determine the effect of vegetation changes on water yield and evapotranspiration, J. Hydrol., 55, 3–23, 1982.

Chen, J. F. and Li, X. B.: Simulation of hydrological response to land-cover changes, Chinese J. Appl. Ecol., 15(5), 833–836, 2004.

Hibbert, A. R.: Forest treatment effects on water yield, in: International Symposiun on Forest Hydrology, edited by: Sopper, W. E. and Lull, H. W., Pergramon, Oxford, p. 813, 1967.

Hollis, G. E.: The effect of urbanization on flood of different recurrence interval, Water Resour. Res., 11(3), 431–435, 1975.

Hu, C. Q.: Computational method of runoff generation in semi-humid and semi-arid regions, Proceedings of the Symposium on Hydrological Information and Forecasting, China Water Power Press, Beijing, China, 57–62, 1993 (in Chinese).

Falkenmark, M. and Rockstrom, J.: Balancing water for humans and nature: the new approach in ecohydrology, Earthscan, UK and USA, 2004.

FAO: World agriculture: Towards 2010, An FAO study, Food and Agriculture Organization, Rome, 1995a.

FAO: Land and water integration and river basin management, Proceedings of an informal workshop 31 Jan–2 Feb 1993, Land and Water Bulletin, Food and Agricultural Organization, Rome, 1995b.

FAO: Food production: the critical role of water, World Food Summit, Technical Background Document7, Food and Agriculture Organization, Rome, 1997.

Li, K. Y., Coe, M. T., Ramankutty, N., and De Jong, R.: Modeling the hydrological impact of land-use change in West Africa, J. Hydrol, 337, 258–268, 2007.

Lorup, J. K., Refsgaard, J. C., and Mazvimavi, D.: Assessing the effect of land use change on catchment runoff by combined use of statistical tests and hydrological modeling: case studies from Zimbabwe, J. Hydrol., 205, 147–163, 1998.

Martz, W. and Garbrecht, J.: Numerical definition of drainage network and subcatchment areas from digital elevation models, Comput. Geotech., 18(6), 747–761, 1992.

Mo, X., Liu, S., Lin, Z., and Zhao, W.: Simulating temporal and spatial variation of evapotranspiration over the Lushi basin, J. Hydrol., 285, 125–142, 2004.

Ott, B. and Uhlenbrook, S.: Quantifying the impact of land-use changes at the event and seasonal time scale using a process-oriented catchment model, Hydrol. Earth Syst. Sci., 8, 62–78, 2004, http://www.hydrol-earth-syst-sci.net/8/62/2004/.

Ren, L., Zhang, W., Li, C., and Wang, M.: Impacts of human activities on river runoff in north China, Journal of Hohai University, 29(4), 13–18, 2002.

Ren, L., Zhang, W., Li, C., Yuan, F., Yu, Z., Wang, J., and Xu, J.: Comparison of runoff parameterization schemes with spatial heterogeneity across different temporal scales in semi-humid and semi-arid regions, J. Hydrol. Eng., 13(5), 400–409, 2008.

Siriwardena, L., Finlayson, B. L., and McMahon, T. A.: The impact of land use change on catchment hydrology in large catchments: The Comet River, Central Queensland, Australia, J. Hydrol., 326, 199–214, 2006.

Shuttleworth, W. J.: Evaporation, in: Handbook of Hydrology, edited by: Maidment, D. R., McGraw-Hill, New York, 4.1–4.53, 1993.

Wilk, J., Andersson, L., and Plermkamon, V.: Hydrological impacts of forest conversion to agriculture in a large river basin in northeast Thailand, Hydrol. Process., 15, 2729–2748, 2001.

Yuan, F.: Hydrological process modeling considering the effect of vegetation, Ph.D. thesis, Hohai University, China, 2006.

Yuan, F., Ren, L., Yu, Z., and Xu, J.: Potential evapotranspiration computation using a two-source method for the Xin'anjiang hydrological model, J. Hydrol. Eng., 13(5),305–316, 2008.

Zhang, L., Dawes, W. R., and Walker, G. R.: Predicting the Effect of Vegetation Changes on Catchment Average Water Balance, Cooperative Research Centre for Catchment Hydrology, Technical Report 99/12, 35 pp., 1999.

Zhao, R. J.: The Xianjiang model applied in China, J. Hydrol., 135(3), 371–381, 1992.

Zhao, R. J., Zhang, Y. L., Fang, L. R., Liu, X. R., and Zhang, Q. S.: The Xinanjiang model, Proceedings of the Oxford Symposium on Hydrological Forecasting, IAHS Pub. No. 129, IAHS Press, Wallingford, UK, 351–356, 1980.

Table 1. Calibrated parameter values for the daily runoff simulation.

	1964–1979	1980–1989	1990–1999	2000–2005
WUM (mm)	20	20	20	20
WLM (mm)	80	80	80	80
WDM (mm)	40	40	40	40
b	0.22	0.17	0.25	0.16
BX	0.25	0.32	0.2	0.15
f_0c (mm/h)	21	20	23	30
f_c (mm/h)	3	3	3	3
k	0.2	0.39	0.18	0.1
k_g	0.88	0.94	0.94	0.92
K_e (hr)	25	26	27	27
X_e	0.26	0.33	0.15	0.16

* WUM, WLM and WDM are tension water capacities of upper, lower and deeper layer, respectively; b is the exponential of tension water storage capacity curve; BX is the shape parameter of infiltration quantity cure; f_0 is the maximum infiltration rate; f_c the static infiltration constant at a surface point; k is decay coefficient with time; k_g is recession constant of groundwater storage; and K_e and X_e are parameters of the Muskingum-Cunge method.

Table 2. Model performance during different period.

Period	1964–1979		1980–1989		1990-1999		2000–2005	
	1964 to 1973 (calibration)	1974 to 1979 (validation)	1980 to 1985 (calibration)	1986 to 1989 (validation)	1990 to 1995 (calibration)	1996 to 1999 (validation)	2000 to 2003 (calibration)	2004 to 2005 (validation)
Q_{obs}(mm)	408.11	311.26	86.03	105.72	314.84	131.38	26.51	32.19
Q_{sim}(mm)	399.69	321.98	73.95	117.06	340.09	121.27	55.53	31.98
Bias (%)	−2.06	3.45	−14.04	10.73	8.02	−7.69	109.5	−0.64
DC	0.685	0.739	0.587	0.639	0.29	0.637	−0.592	0.867

* Q_{obs} is the observed discharge; Q_{sim} is the simulated discharge; *DC* is the Nash-Sutcliffe efficiency; Bias is the relative error.

Table 3. Land use and land cover in variation in Laohahe Catchment, 1964–2005.

Classification	Percentage (%)			
	1980	1989	1996	1999
Forest land	25.9	16.9	31.6	10.5
Grass land	29.1	66.8	16.1	46.5
Crop land	42.7	16.1	48	42.9
Urban	0.6	0.2	1.9	0.1
Others	1.7	0	2.4	0

Table 4. Mean annual potential evapotranspiration under 4 land cover scenarios during different periods (Unit: mm).

Period		Land cover scenario			
		1980	1989	1996	1999
1964–1979	E_i	40.1	36.8	58.4	39.1
	E_{pc}	135.5	118.2	204.8	138.2
	E_{ps}	563.8	581.5	490.1	557.1
	PET	739.4	736.5	753.3	734.4
	E_a	423.2	423.8	427.2	422.5
1980–1989	E_i	38.0	34.5	55.4	37.0
	E_{pc}	133.9	117.9	202.0	135.7
	E_{ps}	571.9	590.6	498.3	566.8
	PET	743.7	742.9	755.8	739.4
	E_a	392.3	392.9	394.6	392.3
1990–1999	E_i	39.5	35.9	57.9	38.0
	E_{pc}	136.8	118.6	205.9	139.2
	E_{ps}	564.1	584.3	487.9	558.7
	PET	740.3	738.9	751.6	735.9
	E_a	445.9	446.5	449.4	445.0
2000–2005	E_i	35.0	31.8	51.5	33.9
	E_{pc}	130.0	114.5	195.1	131.1
	E_{ps}	583.9	604.9	507.9	580.2
	PET	748.9	751.2	754.8	745.2
	E_a	399.6	400.0	401.1	399.6

Table 5. Simulated mean annual runoff during each period under the 4 land cover scenarios.

Period	Item	Land cover map			
		1980	1989	1996	1999
1964–1979	Surface runoff (mm)	7.23	7.22	6.91	7.30
	Groundwater runoff (mm)	37.86	37.22	34.25	38.41
	Total runoff (mm)	45.10	44.45	41.17	45.73
	Runoff ratio	0.0981	0.0967	0.0896	0.0995
1980–1989	Surface runoff (mm)	3.98	3.95	3.69	4.05
	Groundwater runoff (mm)	15.66	15.14	13.72	15.54
	Total runoff (mm)	19.64	19.10	17.41	19.60
	Runoff ratio	0.0473	0.0460	0.0419	0.0472
1990–1999	Surface runoff (mm)	2.95	2.95	2.82	2.99
	Groundwater runoff (mm)	46.78	46.18	43.30	47.60
	Total runoff (mm)	49.75	49.14	46.14	50.61
	Runoff ratio	0.1000	0.0987	0.0927	0.1017
2000–2005	Surface runoff (mm)	0.78	0.78	0.76	0.79
	Groundwater runoff (mm)	13.70	13.34	12.69	13.80
	Total runoff (mm)	14.49	14.13	13.45	14.59
	Runoff ratio	0.0342	0.0334	0.0318	0.0345

Table 6. Annual mean precipitation and runoff during those 4 periods.

	1964–1979	1980–1989	1990–1999	2000–2005
Precipitation (mm)	459.7	408.3	497.5	423.2
Observed Runoff (mm)	44.96	19.17	44.61	9.78
Runoff ratio	0.0978	0.0470	0.0897	0.0231

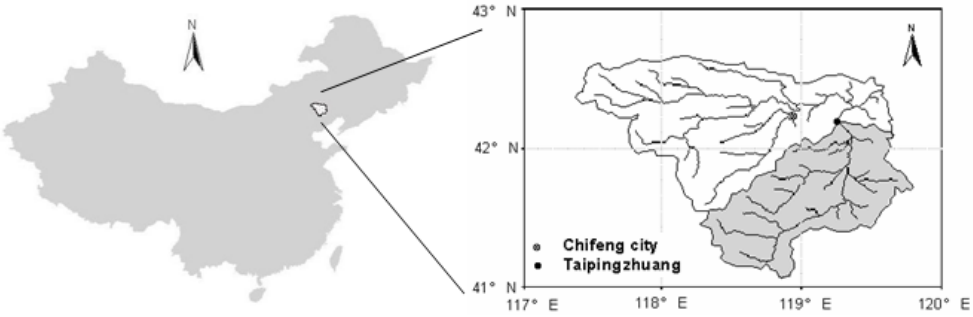

Fig. 1. The location of Laohahe Catchment.

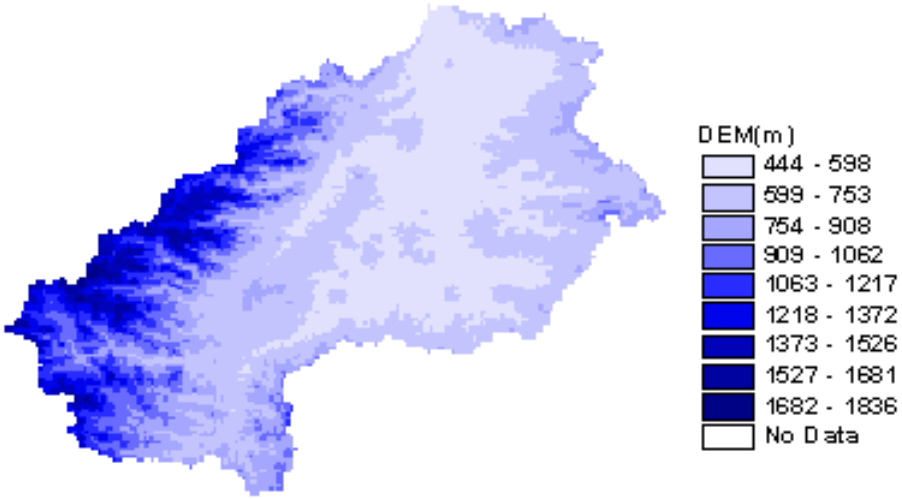

Fig. 2. Digital elevation map of the studied area.

HESSD

5, 2425–2457, 2008

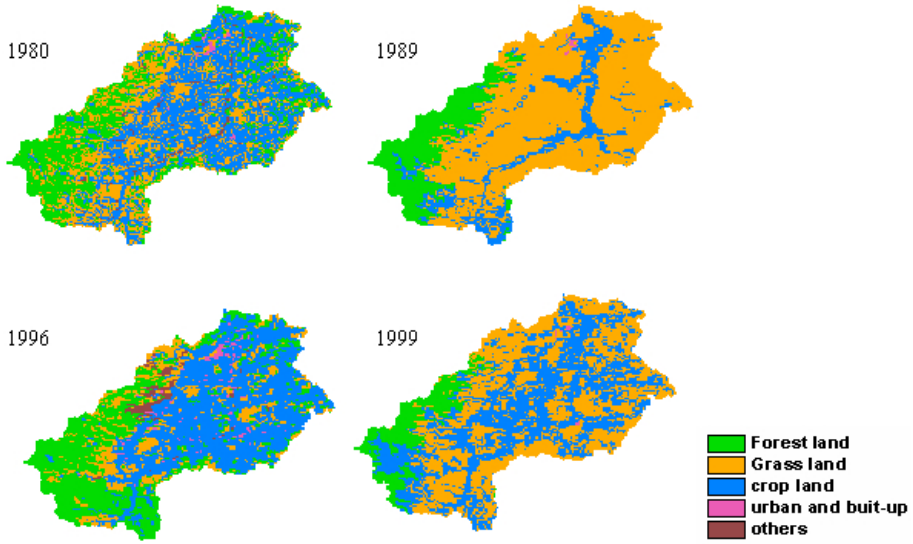

Fig. 3. Four land cover maps in Laohahe Catchment.

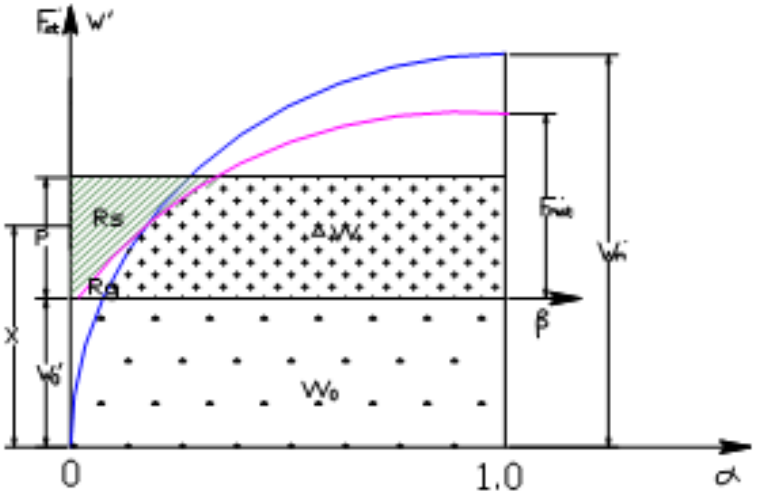

Fig. 4. Basic concept of the hybrid runoff model.

HESSD
5, 2425–2457, 2008

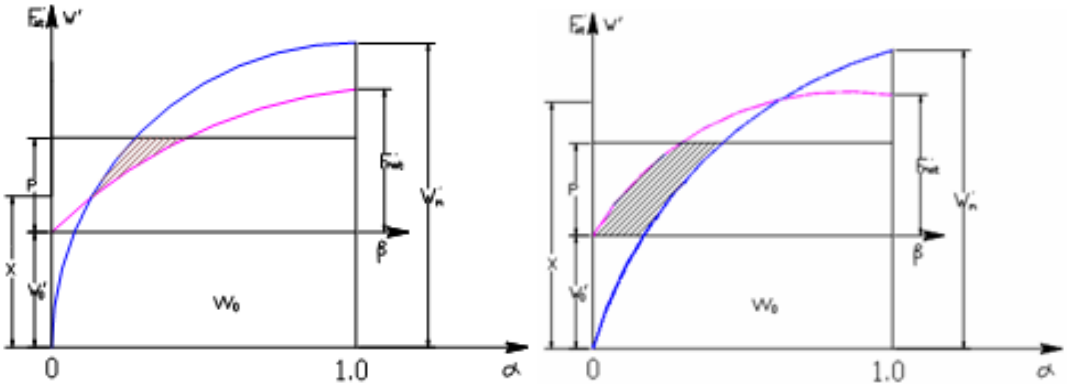

Fig. 5. Two examples explaining the concept of HYB: **(a)** Surface runoff is produced over the partial area (shaded) before soil moisture reaches field capacity because rainfall intensity exceeds the infiltration rate; **(b)** Interflow or groundwater runoff is produced over the partial area (shaded) before rainfall intensity exceeds infiltration rate because soil moisture reaches field capacity.

HESSD

5, 2425–2457, 2008

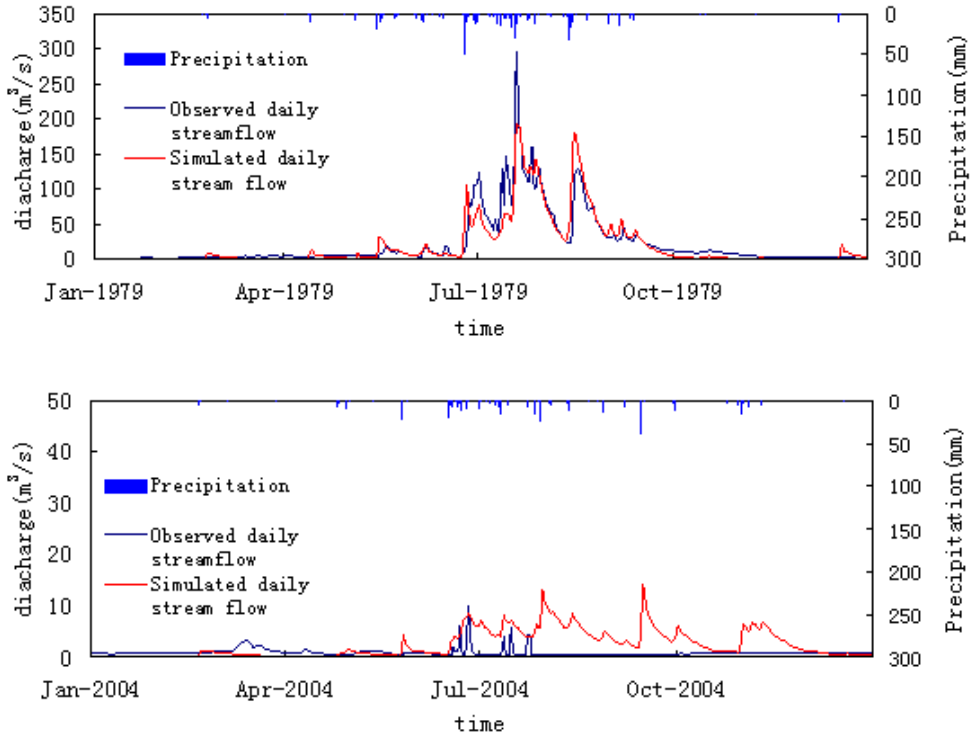

Fig. 6. Comparison of the observed and simulated daily streamflow at the Taipingzhuang station.

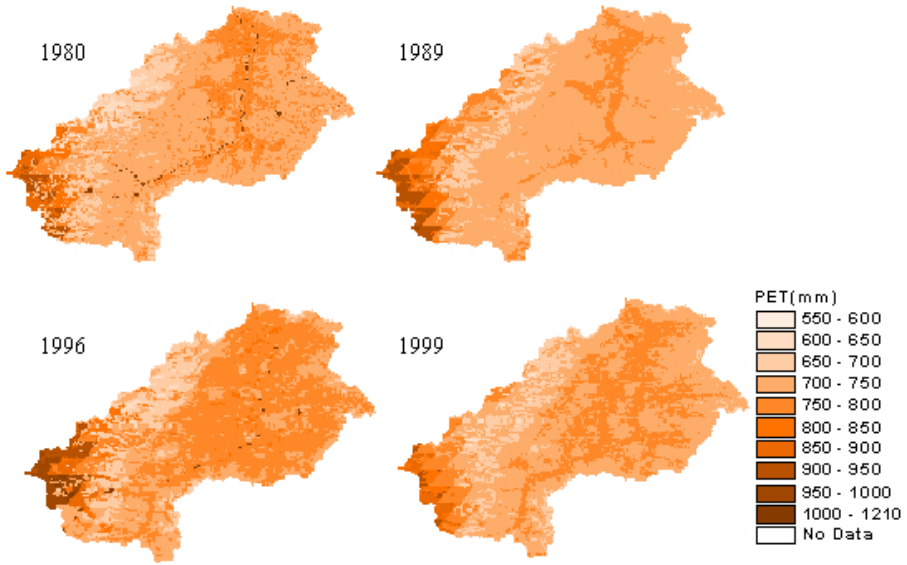

Fig. 7. Spatial distribution of mean annual potential evapotranspiration over the period of 1980–1999 under 4 land cover scenarios.

HESSD
5, 2425–2457, 2008